

A facile fabrication of hydroxyapatite in vitro using polymer fasciculus as biotemplate carrier

Tao Yan, Dong Wei, Xianpeng Zheng, Xiaodong Xin, Nuo Zhang, Dan Wu, Liangguo Yan, He Li, Bin Du*, Qin Wei*

Shandong Provincial Key Laboratory of Fluorine Chemistry and Chemical Materials, School of Chemistry and Chemical Engineering, University of Jinan, Jinan 250022, China

*Corresponding author. Tel.: (+86) 531 82765730; Fax: (+86) 531 82765969; E-mail: sdjndxwq@163.com and sdjndxdb@163.com

Received: 10 April 2010, Revised: 30 May 2010 and Accepted: 31 May 2010

ABSTRACT

For biomimetic synthesis of hydroxyapatite by simulating biomineralization, the polyamide 66 (PA 66) was used as biotemplate carrier, and the biotemplate was prepared by the adsorption of AOT surfactants at interfaces of polymer fasciculus. Simulating biomineralization was carried out at physiological condition ($\text{pH} = 7.4$, $T = 37^\circ\text{C}$). The phase components, morphologies and possible growth mechanism of calcium phosphate were studied by fourier transform infrared spectroscopy (FTIR), transmission electron microscopy (TEM) and scanning electron microscopy (SEM). The results indicated that the course of crystal growth, as well as the morphology and composition of product was markedly dependent on biotemplate; the crystals size were within nanometer scope, with a sphere and short rod-like shape extraordinary close to natural bone. The possible mechanism of crystal growth was discussed. Copyright © 2010 VBRI press.

Keywords: Biomineralization; hydroxyapatite; polymer fasciculus; biomimetic synthesis



Tao Yan received the master's degree from University of Jinan in 2007. His main research interests are biomineralization and environmental chemistry. He published some articles in *Journal of Analytical Chemistry (Russian)*, *Chem. Anal. (Warsaw)*, and *Spectroscopy and Spectral Analysis* etc.



Xianpeng Zheng studies in school of chemistry and chemical engineering, University of Jinan as postgraduate student. He published some articles in *Spectroscopy Letters* and *16th International Symposium on Bioluminescence and Chemiluminescence (2010)*, and so on.



Dong Wei studies in school of resources and environment, University of Jinan as postgraduate student. He published some articles in *Advanced Materials Research* and *International Symposium on Bioluminescence and Chemiluminescences*, and so on.



Xiaodong Xin studies in School of Resources and Environment, University of Jinan as postgraduate student. Some of her articles have been accepted in *Biosensors & Bioelectronics* and *Environmental Technology*, and so on



Nuo Zhang studies in school of chemistry and chemical engineering, University of Jinan as postgraduate student. She has published many articles in *Spectroscopy Letters* and *Spectroscopy and Spectral Analysis*, and so on.



Dan Wu received the D.S. degree from Shandong University in 2005. She dedicates to the surfactant and biological macromolecules interaction. And now she also studies the role of surfactant in electrochemical immunosensor.



Lianguo Yan received the PhD degree from Chinese Academy of Sciences in 2007. His research interest is environmental chemistry.



He Li, Associate Professor, received the Ph.D. degree from Chinese Academy of Sciences, China, in 2004. Since 2009 he has been a Postdoctoral research fellow at University of Wisconsin (USA). His main research interests are biosensor and nanomedicine. He published over thirty articles in *Biomaterials*, *Biosensors & Bioelectronics*, and *Macromolecular Bioscience* etc.



Bin Du, a Professor and DSc, doctoral supervisor, has been engaged in analytic chemistry and environmental science research. He has been investigating deeply the composition, property and application of microemulsion.



Qin Wei, Professor, received the D.S. degree from Chinese Academy of Sciences. She also received the honorary titles of National Teaching teacher, the national outstanding teacher, Shandong Province Outstanding Young Expert and so on, and has completed the study of twelve projects such as national, provincial science fund and doctoral fund. She published over one hundred articles in *Talanta* and *Biosensors & Bioelectronics* etc. In addition, she is a member of the editorial board for several international journals, for instance, *Advanced Materials Letters* and *Spectroscopy and Spectral Analysis*.

Introduction

Calcium phosphates have been widely studied for bone replacement, dental defect filling, bone tissue engineering and drug delivery applications due to their exceptional mechanical properties, excellent biocompatibility and bioactivity [1-3]. Hydroxyapatite $[\text{Ca}_{10}(\text{PO}_4)_6(\text{OH})_2]$, HAP was the most stable calcium phosphate salt. Synthetic HAP particles were similar to the inorganic part of human bones and teeth in structure and size and they were especially studied for biomaterials as reinforcement of polymer and coating of metal [4, 5]. The preparation of HAP phases could be done by a number of novel methodologies such as solution processes, hydrothermal systems, bio-mimetic systems, sol-gel methods and so on [2, 6, 7-17].

Biom mineralization was a natural process in human beings and animals resulting in the formation of bones and teeth. In this process, lots of macromolecules as biotemplate took part in and played an important role in controlling the crystal growth of HAP [18-20]. Biomimetic synthesis of HAP was defined as a method in which a biologically active apatite layer was formed on a matrix after immersion in an artificially prepared supersaturated calcium and phosphate solution [21]. Moreover, biom mineralization was introduced to prepare calcium phosphate during the process. There was a great deal of interest in the study of the solution crystallization pathways of HAP, both from a technological point of view, and from a fundamental perspective aiming at understanding some of the biom mineralization processes. It was usually accepted that the precipitation mechanism of HAP followed a nucleation / aggregation / growth sequence of events [22].

Recently, with the rapid development of the research on the nano-size HAP materials, the molecular control of inorganic crystallization by organic substances has received increasing attention and has been a key technology for the fabrication of novel composite materials [23]. It was observed that the inorganic crystal nucleation and growth depend on the biotemplate assembled by the organic molecule and the biotemplate instructing effect [24, 25]. Some studies showed that the nucleation and growth of HAP crystal could be achieved in many porous and complicated carriers, so the preparation of biotemplate should be considered crucial for the biomimetic synthesis process [26-28]. Therefore, it was vital to prepare biotemplate for the simulating of biom mineralization process in vitro.

In the present work, the biotemplate was prepared using inexpensive polymer fasciculus (PA 66) as carrier by the adsorption of surfactant (AOT) on polymer fasciculus. The biom mineralization process was simulated in vitro by controlling the physiological condition ($\text{pH} = 7.4$, $T = 37^\circ\text{C}$) in order to synthesize HAP nanocomposites. The FTIR spectroscopy was used to analyze the characteristic of biotemplate; the component, morphology of the phase and the possible growth mechanism were studied by means of attenuated total reflection fourier transform infrared spectroscopy (ATR FTIR), scanning electron microscopy (SEM), transmission electron microscopy (TEM),

thermogravimetric analysis (TGA). The emphasis was placed on the characterization of the resulted crystals.

Experimental

Reagents

The macromolecule polymer fasciculus was Peng Hua Polyamide 66 (PH-PA66), from Jinan Juda Fiber Corporation Ltd. in China. The surfactant di-2-ethyl-1-hexyl sulfosuccinate (AOT) was bought from Fluka (Switzerland). All reagents used were of analytical grade purity ($\geq 99.7\%$), supplied by Qiguang Chemicals Company of China. Additionally, doubly distilled water was used throughout this experiment.

Preparation of biotemplate

The polymer fasciculus carriers were ultrasonically cleaned in alcohol for 10 min, in acetone for 15 min, and in distilled water for 5 min sequentially to eliminate the chemical additives. After drying in air, the as-pretreated polymer fasciculus was placed in conical flask which contains AOT solution, and the proportion of adsorbate and adsorbent was kept at 200. Then, the conical flask was placed on a platform shaker (WSZ-100A, Shanghai, Yiheng Technology Co. Ltd.) of 120 rpm. The concentration of AOT was determined by spectrophotometry, and the absorbance was measured using Lambda 35 spectrometer (Perkin Elmer, America). The overall experimental setup is shown in **Fig. 1**.

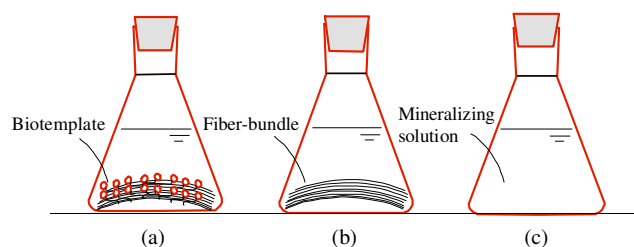


Fig. 1. The advanced project of simulating biomineralization, a) AOT-PH-PA66; b) PH-PA66; and c) Blank mineralizing solution.

Preparation of mineralizing solution

A metastable supersaturated solution was prepared under stirring by mixing the solution of containing Ca and P. 40.0 mL of 0.10 M CaCl_2 stock solution was dissolved in 500 mL volumetric flask, 18.0 mL of 0.10 M Na_2HPO_4 and 12.0 mL of 0.05 M NaH_2PO_4 were mixed and diluted to 500 mL. Then, the solution containing Ca was added to the solution containing P and the pH was adjusted to 7.4 using 0.05 M KOH solution. Meanwhile, 0.1 mol NaCl was dissolved to increase the stability of the supersaturated solution. The concentration of various ions was shown in **Table 1**.

Simulating biomineralization

The mineralizing experiment was carried out illustrated as Figure 1. 1.0 g AOT-PH-PA66 (the polymer fasciculus that adsorbed surfactant) and 1.0 g PH-PA66 (the blank polymer fasciculus) were placed in two conical flasks containing 200 mL mineralizing solution, respectively.

Then, the conical flasks were placed in constant temperature incubator shaker (HZQ-F160A, Shanghai, Yiheng Technology Co. Ltd.) at 37 °C, controlling the shaking rate of 90 rev./min. The pH values were measured with a numeric acidity meter (PHS-3C, Shanghai REX Instrument Factory).

After that, the samples were thoroughly washed with 4% NH_4Cl and distilled water respectively to eliminate residual Ca^{2+} , Na^+ , K^+ , etc. and then dried in air. The blank experiment was also performed (given the name group c) to verify the effect of biotemplate in the heterogeneous nucleation of calcium phosphate phases. The process of deposition experiment was operated as described above.

Table 1. The initialized concentration of ions in mineralizing solution

Ion	Ca^{2+}	Na^+	Cl^-	HPO_4^{2-}	H_2PO_4^-
Concentration (mmol·L ⁻¹)	4.0	104.2	108	1.8	0.6

Characterizations

ATR-FTIR spectroscopy: The polymer fasciculus that has adsorbed AOT was characterized via an FTIR microscope (Perkin-Elmer, FTS-165) with ATR appurtenance. Scans were repeated 16 times with a resolution of 8 cm^{-1} and the region was 4000 - 650 cm^{-1} .

Scanning electron microscopy (SEM): A scanning electron microscope (Hitachi S-2500, 25 kV), equipped with energy dispersive spectroscopy (EDS, LinkISIS-300), was utilized to analyze the morphology, compositions and distribution of mineral on the surface of polymer fasciculus, which were sputtered with gold before observation.

FTIR spectroscopy: The Ca-P deposition was dissolved into alcohol and cleaned with an ultrasonic vibrator for 15 min in order to eliminate residual surfactants. The mineral crystal was separated from solution with centrifuge and dried at room temperature. The calcium phosphate precipitated in blank mineralizing solution also was collected by centrifugation and dried at 50 °C for 48 h. FTIR was used to analyze samples using KBr pellet technique.

Transmission electron microscopy (TEM): The Ca-P deposition collected from biotemplate interface was grinded into powder and suspended in absolute alcohol. After 10 min of ultrasonic dispersion, the drops of the suspension were placed on electron microscope copper grids that formvar-coated and carbon-reinforced. After air-drying, the samples were observed under a transmission electron microscopy (JEM - 100CX II) at 200 kV.

X-ray diffraction (XRD): The XRD measurement was performed on an X'pert Pro rotatory diffractometer (PANalytical) operating at 30 mA and 45 kV using $\text{Co K}\alpha$ as radiation source ($\lambda = 0.1790 \text{ nm}$). The data of 2θ from 10 to 50 ° were collected at a step size of 0.033 °.

Thermogravimetric analysis (TGA): Thermogravimetric analysis was performed in a PerkinElmer Pyris Diamond TG/DTA analyser between 20 and 1100 °C in air at a heating rate of 10 °C/min.

Results and discussion

The optimal conditions of biotemplate preparation

ATR-FTIR analysis: Subtractive infrared spectrum as a novel FTIR technique was applied in the analysis of biotemplate preparation in order to prove the surfactant has been adsorbed on the surface of polymer fasciculus. ATR-FTIR spectra of the polymer fasciculus in **Fig. 2b** that adsorbed AOT surfactant was subtracted from that of the sample prior to adsorption in **Fig. 2a**, the results of which were displayed in **Fig. 2c**. The absorption bands at 2922 and 2850 cm^{-1} were attributed to the vibration absorption of alkyl. The stretching vibration peaks of $-\text{NH}-$ were examined at 3297 cm^{-1} . The band at 795 cm^{-1} was attributed to the stretching mode of $\text{C}-\text{S}$. The bands at 1021 and 1097 cm^{-1} were ascribed to the symmetric stretching vibration of $\text{S}=\text{O}$; the bands at 1163 and 1370 cm^{-1} corresponded to the characteristic adsorption of $-\text{SO}_3^-$. These observations imply that the AOT surfactant (contains $-\text{SO}_3^-$) was adsorbed on the surface of polymer fasciculus.

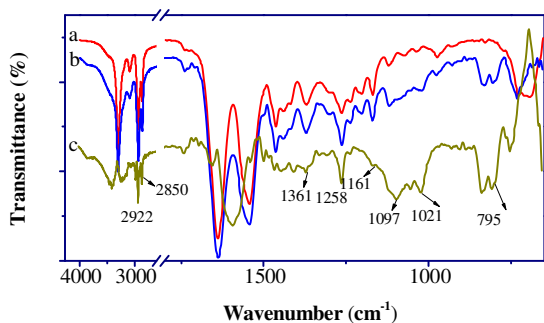


Fig. 2. ATR-FTIR spectrum and subtractive infrared spectrum, a) PH-PA66; b) AOT-PH-PA66; and c) Subtractive infrared spectrum.

Effect of adsorption time: The adsorption capacity and adsorption time curve were shown in **Fig. 3**. It could be seen that the adsorption time has a great effect on the adsorption capacity. When the time was in the range of 1 ~ 7 hours, the concentration of AOT declined obviously, suggesting that the adsorption quantity of AOT on PH-PA66 enhanced clearly. Subsequently, with the increase of time (7 ~ 13 h), the concentration of AOT decreased slowly, and when the adsorption time reached 13 h, the adsorption quantity of AOT on PH-PA66 kept unchanged. Thus, 13 h was chosen as the adsorption time in subsequent experiments.

Adsorption isotherm: According to above procedure, the adsorption time was fixed at 13 h and the proportion of adsorbate and adsorbent was kept at 200, then the adsorption isothermal curve was obtained by varying concentration of AOT solution. The result given in **Fig. 4** showed that the saturated adsorption quantity of AOT on

polymer fasciculus was affected by the initial concentration of adsorbate. The isotherm shows a sharp initial rise, which can be attributed to the driving force of the concentration gradient because an increase of AOT concentration accelerate the diffusion of AOT from the solution onto adsorbent. When the initial concentration of AOT was 0.4 $\text{g}\cdot\text{L}^{-1}$, the adsorption equilibrium can be reached, leading to the maximum saturated adsorption quantity. This value can be kept constant as the initial concentration of AOT was increased to a further degree. Thus, 0.4 $\text{g}\cdot\text{L}^{-1}$ AOT solution was selected as the optimal concentration of adsorbate.

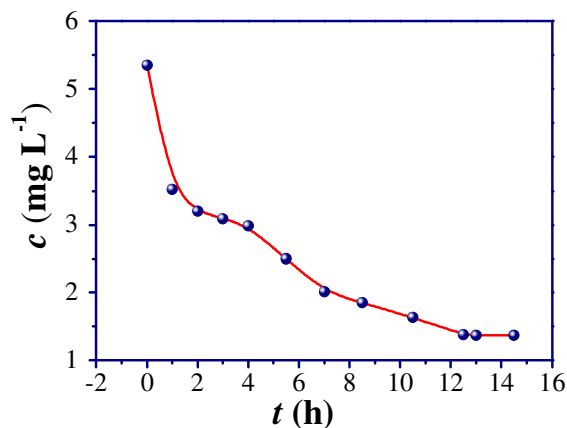


Fig. 3. Effect of time on the adsorption of AOT on PH-PA66

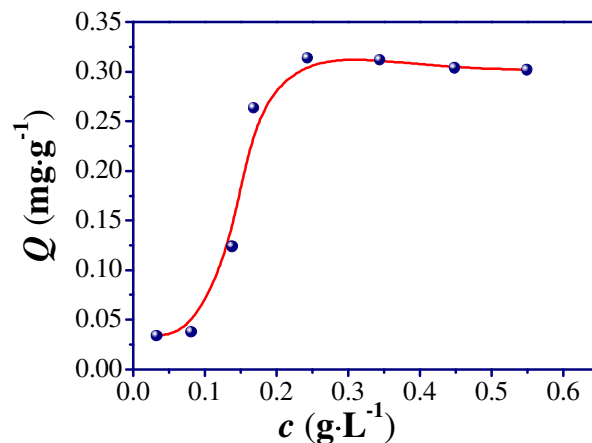


Fig. 4. Adsorption isotherm of AOT by PH-PA66

Process Monitoring of simulating biomineralization

The calcium phosphate deposition can be explained with the decrease of the pH value. **Fig. 5** depicts the time dependence on pH values during the mineralizing process. For the mineralizing solution containing polymer fasciculus that adsorbed AOT (**Fig. 5a**), the pH value exhibited a relatively rapid drop because of distinct induction of biotemplate on the nucleation of mineral. Unlikely, for the solution containing blank polymer fasciculus (**Fig. 5b**), the pH value decreased slowly. This is possibly because the declining of activation energy of nucleation due to the increase of the contact area of solid/liquid surface, thus leading to the heterogeneous

nucleation process occurred spontaneously. The deposition did not happen in the solution containing only blank mineralizing solution as control sample (Fig. 5c). Some precipitates appeared on the beaker and suspended in the solution, the pH value decreased slightly due to the definite supersaturation and buffer ability of the mineralizing solution. The ionization and hydrolyzation process did not achieve equilibrium when the pH value was 7.4, resulting in the further decrease of pH value of the solution.

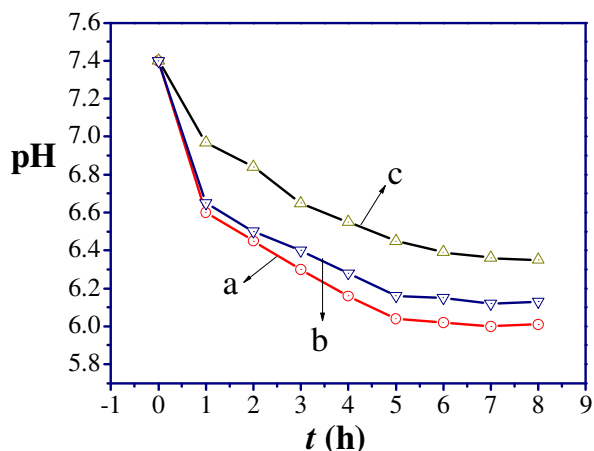


Fig. 5. Changeable curve of pH with time of different systems, a) AOT-PH-PA66; b) PH-PA66; and c) Blank mineralizing solution.

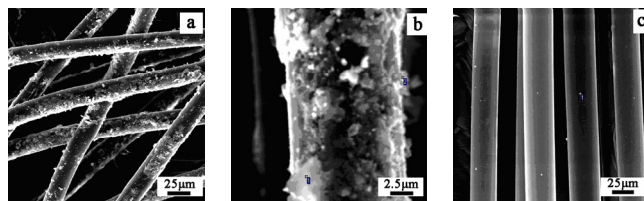


Fig. 6. SEM photograph of samples, a) AOT-PH-PA66, 500 times; b) AOT-PH-PA66, 3000 times; and c) PH-PA66, 500 times.

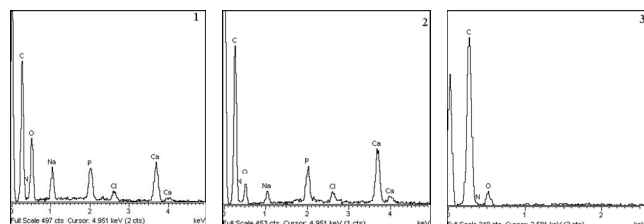


Fig. 7. Energy spectrum of point 1, 2 and 3 in the SEM photograph of b, c.

Characterization of biomineralization products

SEM and EDS analysis: SEM photographs of the polymer fasciculus soaked in mineralizing solution for 48 h were shown in Figure 6. From Fig. 6(a) and (b), it can be seen that the surface of AOT-PH-PA66 polymer fasciculus was covered with white crystals and a compact mineral layer

was formed, which were aggregates of nano-crystallites. In Fig. 6(c), a small quantity of mineral crystal appeared on the surface of blank polymer fasciculus, because the activation energy of heterogeneous nucleation of calcium phosphate phases has been reduced greatly due to definite supersaturation of mineralizing solution.

For a further investigation on the composition of the mineral products, the EDS were performed on selected samples. The results were shown in Fig. 7 and Table 2. It is suggested that the mineral products were mostly composed of Ca and P elements, and also contained Na and Cl elements (The Na^+ and Cl^- that adsorbed on the surface of sample were eliminated by cleaning, and the C, N, O elements came from the polymer fasciculus). From element analysis results, it can be seen that the Ca/P ratio of the crystals in group a was in the range of 1.56 ~ 1.67, which is close to the theoretical value of HAP ($\text{Ca/P} \approx 1.67$). The slightly lower absolute value was possibly due to the Ca^{2+} defect or the lattice substitution of other ions (such as Na^+ , CO_3^{2-}), resulting from the competitive nucleation behavior of various ions on the surface of biotemplate.

Table 2. Element analysis of point 1, 2 and 3 in the SEM photograph of b and c.

Element	Group 1		Group 2		Group 3	
	Point 1	Point 2	Point 2	Point 3	Point 3	Point 3
	Wt. %	At. %	Wt. %	At. %	Wt. %	At. %
C K	41.56	51.46	52.94	64.50	77.87	82.30
N K	14.40	15.20	15.23	15.91	1.22	1.10
O K	28.89	26.69	12.87	12.88	20.91	16.59
Na K	3.29	2.12	1.41	0.90		
P K	3.81	1.82	4.27	2.02		
Cl K	1.18	0.49	1.40	0.58		
Ca K	6.87	2.53	11.88	3.23		
Totals	100.00		100.00		100.00	
Ca/P		1.56		1.60		

FTIR analysis: EDS only told us calcium and phosphorous existed, without the ability to distinguish various calcium phosphates. FTIR was a good tool for structural investigations on the basis of the theory about the vibration origins of diversified chemical bond. As shown in Figure 8(a), FTIR spectrum of the Ca-P deposition in groups a exhibits sharp and well-resolved peaks at 950~1100 and 550~650 cm^{-1} which are the characteristic of a well crystallized apatite phase [29, 30]. The peaks at 1032 and 1093 cm^{-1} were assigned to ν_3 stretching of PO_4^{3-} , two well-separated peaks at 605 and 563 cm^{-1} both assigned to ν_4 mode of PO_4^{3-} and the peaks at 955 and 463 cm^{-1} assigned to ν_1 stretching and ν_2 bending modes of PO_4^{3-} , respectively [31]. The peaks at 1400 ~ 1600 cm^{-1} and 860 ~ 880 cm^{-1} were assigned to the CO_3^{2-} ions in the apatite lattice. These observations can be attributed to the partial substitution of PO_4^{3-} sites by CO_3^{2-} groups in crystal structure [32, 33]. The broad bands at

3400 cm^{-1} and 1638 cm^{-1} were attributed to hygroscopic moisture and O-H stretching vibration of crystals. As a conclusion from above results, the mineral crystals were carbonate-containing hydroxyapatite and the chemical compositions were similar to bone apatite.

Comparing Fig. 8(a) with Fig. 8(b), it can be observed that there is no obvious difference between absorption bands of Ca-P deposition in group b and that of the sample in group a. However, the CO_3^{2-} peaks were more obvious in Fig. 8(a), so the carbonate content appears to be higher in group a. In addition, the H_2O peak at 3400 cm^{-1} of spectra (a) was more obvious than that of spectra (b), implying the higher crystallinity of the sample in group a.

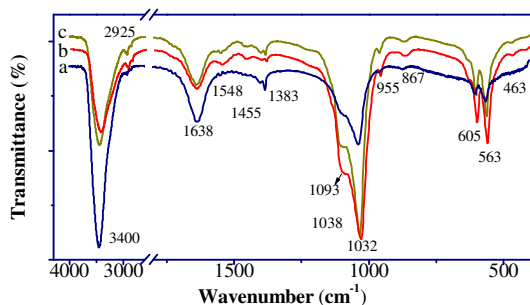


Fig. 8. FTIR spectra of three systems, a) AOT-PH-PA66-HAP, the deposition of biotemplate at 48 h; b) PH-PA66-HAP, the deposition of blank polymer fasciculus at 48 h; and c) Blank mineralizing solution, the precipitate of blank mineralizing solution at 48 h.

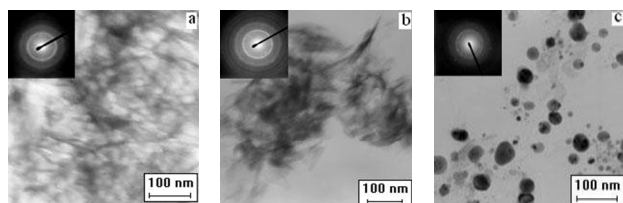


Fig. 9. TEM photographs of samples before and after pre-calcification process a) AOT-PH-PA66; b) PH-PA66; and c) Blank mineralizing solution.

The Ca-P precipitates in blank mineralizing solution (group c) were used as contrasts, seen in Fig. 8(c). From the band-splitting at 1030 ~ 1100 cm^{-1} , it can be immediately observed that the crystallinity of sample (a) and (b) were higher than that of sample (c). The wide and weakened absorption band was composed of the absorption shoulder at 1032 cm^{-1} and the unobvious PO_4^{3-} peak at 955 cm^{-1} , the latter one was the symbol of PO_4^{3-} existing in amorphous calcium phosphate. Moreover, the H_2O peaks in sample (c) were more obvious than those in sample (a) and (b). This indicates that the products collected from blank mineralizing solution were amorphous calcium phosphate (ACP).

TEM analysis: TEM and the selected area electron diffraction (ED) patterns of sample (a), (b) and (c) were shown in Fig. 9. The size and morphology of the as-synthesized products were similar between group 1 and group 2, the products assumed needle-like whiskers or

ribbon-like and elongated crystals growing along the c -axis orientation preferentially with the average diameter of under 100 nm in length. The shape and size of this sample was comparable with the bone apatite producing by physiological biomineralization.

The Electron diffraction (ED) patterns of three systems in Fig. 9(a) and (b) indicated that the products were polycrystalline crystals with different crystallinity. This is similar with the characterization results of EDS (the Ca/P between 1.56 and 1.67). Additionally, at the early age of the mineralization process, the ACP (amorphous calcium phosphate) and OCP (octacalcium phosphate) appeared as the precursors of the samples containing Ca and P, which were accumulated on surface microzone of biotemplate. Then, the referred precursors would be transformed into HAP with the extension of time. The possible reason is that the crystallization kinetics predominate in the mineralization process initially and ultimately the thermodynamic enthalpy.

A little amount of deposition was collected from blank mineralizing solution, the TEM and ED patterns of which are illustrated in Fig. 9(c). The shape of the compound was close to a sphere. Moreover, the crystallinity of this compound was poor and the characteristic of crystal growth was undefined. It could be interpreted that the blank mineralizing solution itself could not accelerate the crystal nucleation. This result correlates well with that of FTIR analysis.

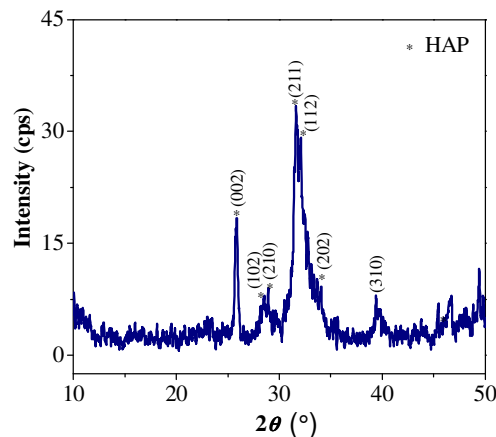


Fig. 10. XRD patterns of HAP crystals of the sample of group a (AOT-PH-PA66).

XRD analysis: The XRD patterns of sample (a) are shown in Fig. 10. It can be seen that characteristic peaks of HAP were observed for the sample. However, by comparing the diffraction data with that in JCPDS database, it can be found that stronger intensity of the corresponding peaks was obtained. Additionally, the typical diffraction peaks at 25.8°, 31.6° and 32.2° were attributed to (002), (211) and (112) crystal planes of HAP phase. This is also different from the assignment according to the standard database, in which the peaks at 31.8°, 32.2° and 32.9° are the characteristic ones of the (211), (112) and (300) crystal

planes of HAP phase. The possible reason is that preferred orientation occurs for the growth of HAP crystal on the surface of polymer fasciculus. Herein, the referred HAP is a columnar or needlelike crystal with hexagon cross-section and *c*-axis is the column axis. Moreover, the size of the HAP crystallite which grows along the *c*-axis was calculated from the line broadening of the d_{002} reflection using Scherrer Equation. 47.2 nm was obtained and this correlates well with the TEM results.

Thermogravimetric analysis (TGA): The profiles of the weight of samples versus different temperatures were determined by thermogravimetric analysis (see **Fig. 11**). It can be seen that three weight loss stages appeared for all the samples. The first stage starts from room temperature to 200 °C, which was assigned to the evaporation of adsorbing water in mineral salts; the second stage from 200 °C to 500 °C was ascribed to the decomposition of residue organic matter; the last stage from 550 °C to 1100 °C was attributed to the decomposition of CO_3^{2-} . It could be seen that the CO_3^{2-} content was 5.3 %, 3.6 % and 13.8 % in three compounds, respectively. Among them, the value of 5.3 % for AOT-PH-PA66 is similar with that in bone apatite, which is reported to be 5.0 ~ 8.0 % according to earlier research.

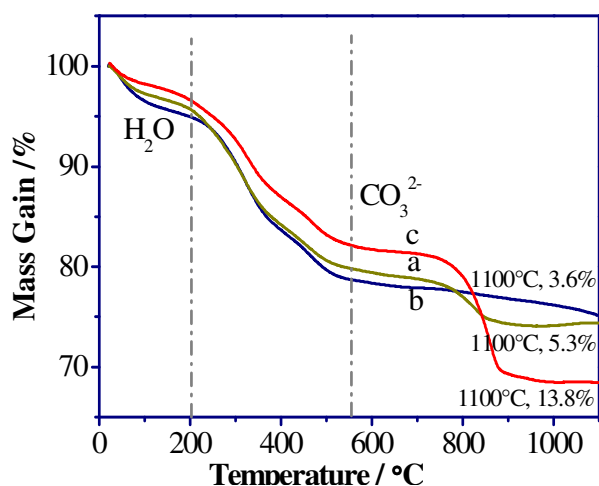


Fig. 11. TG curves of samples, a) AOT-PH-PA66; b) PH-PA66; and c) Blank.

Discussion of biomineralization mechanism

Mann has put forward Boundary-Organized-Biomineralization conception that the biomineralization process was influenced by various factors and the formation of biomineral was due to the synergistic effects of these factors [34]. The experimentation *in vitro* indicated that the formation of apatite-mineral started from the process that the positive ion enriched on electronegative groups of corresponding biomacromolecules [35]. The concentration of Ca^{2+} in surface microzone was independent of bulk concentration. It means that the Ca^{2+} was accumulated in the microzone, the ion concentration was relative and non-stoichiometric in surface microzone. In this experiment, the polar groups of surfactant that face water phase constituted the adsorption layer or surface micellization. Owing to the

excellent inducement ability of hydrophilic groups, positive ions (Ca^{2+} , K^+ , Na^+ , etc.) ions would be preferentially concentrated in template surface microzone as a bridge, promoting the accumulation of electronegative groups such as HPO_4^{2-} , PO_4^{3-} and OH^- by electric charge interaction. In surface microzone of the template, crystal nucleus appeared when the ion concentration exceeded the critical saturation value of mineral crystal. Once the mineral crystal nucleus was formed, the tendency of the process would be the growth of crystal nucleus rather than the formation of new crystal nucleus.

At the beginning, crystal nucleus was stochastic oriented and collided with each other in virtue of Brownian motion. Thus the mineral particulate can get over the repulsive force and then congregated together, leading to the obvious decrease of surface area and surface free energy. That is to say, as a result of the Brownian motion and the short range intermolecular force, the adjacency particulates wobbled slightly until the surface free energy was the lowest. Simultaneously, these particulates accumulated according to the identical crystallization orientation and the mineral crystal was finally formed.

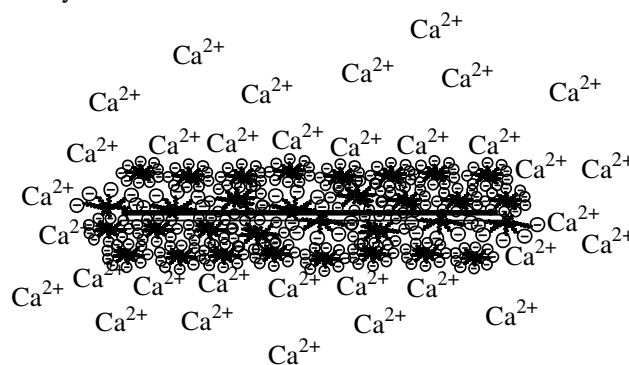


Fig. 12. Sketch of accumulation of Ca^{2+} on the surface of the template

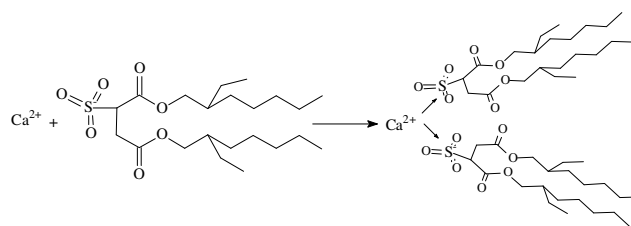


Fig. 13. Sketch of chemical bond between Ca^{2+} and AOT.

There are two functions of Ca^{2+} as a bridge: Firstly, owing to the ionization of appendiculate surfactant molecule and the ion-exchange effects, the positive groups of surfactant molecule can be substituted by Ca^{2+} . It can be used as a complex ion, taking part in the complexation process with polar groups of surfactant molecule. Secondly, Ca^{2+} provided a nucleation site for the mineral crystal, during the process of biomineralization, more and more PO_4^{3-} , OH^- anions were accumulated to the template

surface microzone and promoted the formation of crystal nucleus ultimately (see Fig. 12 and Fig. 13).

Conclusion

In this paper, the simulating biomineralization in vitro was carried out successfully. A biotemplate was prepared by the adsorption of AOT surfactant at interfaces of polyamide 66 and then provided for the ordered fabrication of HAP. SEM results showed that HAP elongated clusters should be composed of nanosized crystallites which were formed on the biotemplate surface. TEM results demonstrated that the HAP was comprised of anisotropic crystallites (≤ 100 nm), which were elongated in the *c*-axis and this was similar to the geometry of bone apatite crystals. FTIR spectroscopy results strongly suggests that the HAP was bonded with the AOT via the sulfonic acid groups and that it was highly likely that the HAP has an octacalcium precursor similar to natural bone apatite. Furthermore, polymer fasciculus was used as novel template carrier materials in the preparation of biotemplate, owing to its inexpensive and common characteristics and its extensive usage in many fields, the proposed method may be developed for further potential applications in many new fields such as water treatment facilities.

Acknowledgements

This study was supported by the Natural Science Foundation of China (20577016), The Natural Science Foundation of Shandong Province (Y2006B36 and Y2008B44), and the Key Subject Research Foundation of Shandong Province (XTD0705), and all the authors express their deep thanks.

References

1. Navarro, M.; Michiardi, A.; Castaño, O.; Planell, J. A. *J. R. Soc. Interface* **2008**, 5, 1137.
2. Viswanath, B.; Ravishankar, N. *Biomaterials* **2008**, 29, 4855.
3. Rey, C.; Combes, C.; Drouet, C.; Sfihi, H.; Barroug, A. *Mater. Sci. Eng. C Biomim. Mater. Sens. Syst.* **2007**, 27, 198.
4. Ban, S.; Maruno, S. *Biomaterials* **1998**, 19, 1245.
5. Cui, F. Z.; Li, Y.; Ge, J. *Mater. Sci. Eng. R-Reports* **2007**, 57, 1.
6. Anee, T. K.; Sundaram, M. N.; Arivuoli, D.; Ramasamy, P.; Narayana, K. S. *J. Cryst. Growth* **2005**, 285, 380.
7. Wang, A.; Liu, D.; Yin, H.; Wu, H.; Wada, Y.; Ren, M.; Jiang, T.; Cheng, X.; Xu, Y. *Mater. Sci. Eng. C* **2007**, 27, 865.
8. Raynaud, S.; Champion, E.; Bernache-Assollant, D.; Thomas, P. *Biomaterials* **2002**, 23, 1065.
9. Liu, J.; Li, K.; Wang, H.; Zhu, M.; Yan, H. *Chem. Phys. Lett.* **2004**, 396, 429.
10. Chen, H.F.; Sun, K.; Tang, Z. Y.; Robert, V. L.; John, F. M.; Agata, C. J.; Clarkson, B. H. *Crys. Growth Des.* **2006**, 6, 1504.
11. Ashok, M.; Narayana Kalkura, S.; Meenakshi Sundaram, N.; Arivuoli, J. *Mater. Sci. Mater. Med.* **2007**, 18, 895.
12. He, Q. J.; Huang, Z. L. *Cryst. Res. Technol.* **2007**, 42, 460.
13. Zhang, X.; Vecchio, K. S. *J. Cryst. Growth* **2007**, 308, 133.
14. , M.; Mitrić, M.; Skapin, S.; Jančar, B.; Ignjatović, N.; Uskoković, D. *Cryst. Growth Des.* **2008**, 8, 2217.
15. Ruban Kumar, A.; Kalainathan, S. *Cryst. Res. Technol.* **2008**, 43, 640.
16. Neira, I.S.; Guitián, F.; Taniguchi, T.; Watanabe, T.; Yoshimura, M. *J. Mater. Sci.* **2008**, 43, 2171.
17. Zhang, H. B.; Zhou, K. C.; Li, Z. Y.; Huang, S. P. *J. Phys. Chem. Solids* **2009**, 70, 243.
18. Koutsopoulos, S.; Dalas, E. *J. Cryst. Growth* **2001**, 222, 279.
19. Zhai, Y.; Cui, F. Z. *J. Cryst. Growth* **2006**, 291, 202.
20. Onuma, K.; Yamagishi, K.; Oyane, A. *J. Cryst. Growth* **2005**, 282, 199.
21. Liu, Q.; Ding, J.; Mante, Francis K.; Wunder, Stephanie L.; Baran, George R. *Biomaterials* **2002**, 23, 3103.
22. Clement, R. R.; Macipe, A. L.; Morales, J. G.; Burgues, J. T.; Castano, V. M. *J. Eur. Ceram. Soc.* **1998**, 18, 1351.
23. Mann, S.; Archibald, D. D.; Didymus, J. M.; Douglas, T.; Heywood, B.R. *Sci.* **1993**, 261, 1286.
24. Tanev, P. T.; Pinnavaia, T. J.; *Sci.* **1996**, 271, 1267.
25. Firouzi, A.; Kumar, D.; Bull, L. M.; besier, T.; sieger, P.; Huo, Q.; walker, S. J.; Zasadzinski, J. A.; Glinka, C.; Nicol, J.; Margolese, D.; Stucky, G. D.; Chmelka, B. F. *Sci.* **1995**, 267, 1138.
26. Mucalo, M. R.; Yokogawa, Y.; Toriyama, M.; Suzuki, T.; Kawamoto, Y.; Nagata, F.; Nishizawa, K. *J. Mater. Sci.: Mater. Med.* **1995**, 6, 597.
27. Hartgerink, J. D.; Beniash, E.; Stupp, S. I. *Sci.*, **2001**, 294, 1684.
28. Liu, J. Z.; Gou, B. D.; Xu, S. J.; Wang, K. *Sci.* **2002**, 12, 615.
29. Xu, G. F.; Aksay, Ilhan A.; Groves, J. T. *J. Am. Chem. Soc.* **2001**, 123, 2196.
30. Xiong, X. B.; Zeng X. R.; Zou, Ch. L.; Li, P.; Fan, Y. B. *Surf. Coat. Technol.* **2009**, 204, 115.
31. Liang, Q.; Han, D. M.; Gu, F. B.; Wang, Zh. H.; Guo, G. *Sh. Chinese J. Inorg. Chem.* **2007**, 23, 86.
32. Filho, O. P.; La Torre, G. P.; Hench, L. L. *J. Biomed. Mater. Res.* **1996**, 30, 509.
33. Wang, X. J.; Li, Y. B.; Wei, J.; Groot, K. D. *Biomaterials* **2002**, 23, 4787.
34. Mann, S. *J. Inorg. Biochem.* **1986**, 28, 363.
35. Heuer, A. H.; Fink, D. J.; Laraia, V. J.; Arias, J. L.; Calvert, P.D.; Kendall, K.; Messing, G. L.; Blackwell, J.; Rieke, P.C.; Thompson, D.H. *Sci.* **1992**, 255, 1098.